3d/4f Coordination clusters as cooperative catalysts for highly diastereoselective Michael addition reactions

Kieran Griffiths,[†] Athanassios C. Tsipis,[‡] Prashant Kumar,[†] Oliver P. E. Townrow,[†] Alaa Abdul-Sada,[†] Geoffrey R. Akien,[§] Amgalanbaatar Baldansuren,[⊥] Alan C. Spivey,[∥] and George E. Kostakis[†]*

† Department of Chemistry, School of Life Sciences, University of Sussex, Brighton BN1 9QJ, UK.
‡ Laboratory of Inorganic and General Chemistry, Department of Chemistry, University of Ioannina, 451 10 Ioannina, Greece.
§ Department of Chemistry, Lancaster University, Lancaster LA1 4YB, UK.
⊥ School of Chemistry, The University of Manchester, Manchester M13 9PL, UK.
∥ Department of Chemistry, South Kensington Campus, Imperial College London, SW7 2AZ, UK.

ABSTRACT: Michael addition (MA) is one of the most well studied chemical transformation in synthetic chemistry. Here, we report the synthesis and crystal structures of a library of 3d/4f coordination clusters (CCs) formulated as $[Zn^{II}_2Y^{III}_2L_4(solv)_X(Z)_Y]$ and study their catalytic properties towards the MA of nitrostyrenes with barbituric acid derivatives. Each CC presents two borderline hard/soft Lewis acidic Zn^{II} centers and two hard Lewis acidic Y^{III} centers in a defect dicubane topology that brings the two different metals into a proximity of ~3.3 Å. DFT computational studies suggest that these tetrametallic CCs dissociate in solution to give two catalytically active dimers, each containing one 3d and one 4f metal which act cooperatively. The mechanism of catalysis has been corroborated *via* NMR, EPR and UV-Vis. The present work demonstrates for the first time the successful use of 3d/4f CCs as efficient and high diastereoselective catalysts in MA reactions.

INTRODUCTION

Nature provides many highly efficient but complex catalytic systems that rely on synergistic, cooperative activation through multiple metal centers. Examples include tyrosinase[1] and photosystem II.[2] To emulate this behavior is hugely challenging and it is only in the last decade that polynuclear coordination clusters (CCs),[3–5] especially ones containing two metals,[6–11] have emerged as viable platforms to achieve this. Bimetallic cooperative catalysts have been described comprising different types of metals encompassing alkali, transition and lanthanides.[12–17] Unsurprisingly, the precise topology of the cluster and in particular the distance separating the two metals (typically 3.5–6 Å) has been suggested to be a key parameter for efficient catalysis.[8] Only a few 3d/4f bimetallic catalysts have been reported, but some of these have been shown to display high diastereo- and enantioselectivity in nitro-Mannich[14,17] and Henry[12] reactions, and excellent efficiency in oxidation of alcohols[18] and water.[19]

We have previously reported the synthesis of a small library of heterometallic 3d/4f CCs possessing a rigid defect dicubane topology, with the general formula $[M^{II}_2Ln^{III}_2(L1)_4(solv)_X(Z)_Y]$ (**1MLn**), where H_2L1, is (*E*)-2-(2-hydroxy-3-methoxybenzylidene-amino)phenol, M is Co/Ni/Zn, Ln is Y[20]/Sm/Eu/Gd/Dy/Tb/Yb, solv is EtOH/CH₃CN/DMF, and Z is Cl/NO₃/ClO₄ (Figure 1).[21–25]

The crystallographic characterization of seven of these CCs containing different metal combinations (*i.e.* **1ZnY**, **1ZnSm**, **1ZnEu**, **1ZnGd**, **1ZnDy**, **1ZnTb** and **1ZnYb**), have been reported previously[23] and reveal that in all cases the 3d and 4f metals are close together (3.3±0.1 Å).
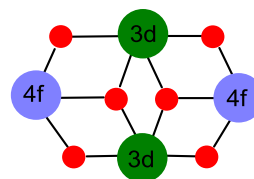
Figure 1. A cartoon representation of a 3d/4f CC. Red balls indicate O atoms.

In addition to developing a facile method for the synthesis of these 3d/4f CCs, and structurally characterizing them, we have previously demonstrated their stability in solution (by ESI-MS, EPR and NMR) and their catalytic competence at room temperature and low catalyst loading (1-2.5 mol%) in 2-furaldehyde/*sec*-amine domino reactions,[21,22] in Friedel-Crafts type indole/aldehyde and indole/nitrostyrene alkylation reactions,[23,24] and in Petasis-Manich reactions.[25] By maintaining the hard 4f center invariant and tuning the 3d center (Co, Ni, Cu, or Zn), we have shown that valuable mechanistic information can be extracted by correlating product distributions and selectivity *vs*. metal properties.[26] Such correlations are not pos-

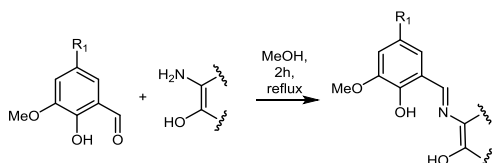sible using homometallic polynuclear 3d/3d or 4f/4f catalysts.

Michael additions (MAs) are some of the most well studied chemical transformation in synthetic chemistry and various catalytic protocols displaying high levels of diastereo- and enantioselectivity have been developed, including those promoted by organocatalysts, simple salts, and complexes.[27–30]

Inspired by Shibasaki's pioneering studies into nitro-Mannich reactions catalyzed by a presumed dinuclear Cu/Sm CC formed *in situ*,[14,17] in which cooperative binding of the substrates to both metal centers was proposed, we envisaged that our library of catalysts might provide efficient catalysts for MA reactions. To this end, we opted to investigate the MA reactions of nitrostyrenes and 1,3-dimethyl barbituric acid as a test system.[31–33] To the best of our knowledge there is no previous report with the use of bimetallic 3d/4f as catalysts in MA reactions. Modification of the ligand and the metal centers as well as *in situ* studies of the catalytic reaction with UV Vis, NMR and EPR spectroscopy have been carried out and the mechanistic insights provided by these methods augmented by DFT computation.

RESULTS AND DISCUSSION

Catalyst Synthesis. Using our already reported ZnY CC **1ZnY** as a starting point, a library of 20 analogous ZnY CCs was prepared using substituted (*E*)-2-(2-hydroxy-3-methoxybenzylidene-amino)phenol ligands (H_2L1-H_2L21, Table 1). These ligands were easily synthesized in one step by condensation of three commercially available 5-substituted-3-methoxysalicylaldehydes (5-H, 5-allyl and 5-Br) with seven 2-aminophenol derivatives, under ambient conditions and in high yields (Table 1).

Table 1. The synthesis and structures of ligands H_2L1- H_2L21 used to prepare CCs **1ZnY-21ZnY**.

R_1							
H	H_2L1	H_2L4	H_2L7	H_2L10	H_2L13	H_2L16	H_2L19
allyl	H_2L2	H_2L5	H_2L8	H_2L11	H_2L14	H_2L17	H_2L20
Br	H_2L3	H_2L6	H_2L9	H_2L12	H_2L15	H_2L18	H_2L21

The selected ligands were expected to offer very similar coordination environments, such that the same core CC motif would assemble and we would be able to identify the influence of the second coordination sphere on their properties as catalysis. The solid CCs were synthesized in one-step reactions using the ligand H_2L, $Zn(NO_3)_2$ $6H_2O$, $Y(NO_3)_3$ $x(H_2O)$ and Et_3N under reflux for 2 hours in excellent yields (>90%). In all cases, compounds formulated as $[Zn^{II}_2Y^{III}_2L_4(NO_3)_2(DMF)_2]$ solvent were obtained and they were characterized by TGA and CHN analysis.

Crystal structures. For nine of the CCs (**2ZnY, 4ZnY, 7ZnY, 8ZnY, 10ZnY, 14ZnY, 15ZnY, 16ZnY and 19ZnY**), crystals suitable for single crystal X-ray diffraction were obtained by the vapor diffusion method using DMF and Et_2O. The crystal structures of all nine clusters are shown below (Figure 2). We use the term "isoskeletal",[34] to describe all these catalysts as they all possess a defect dicubane topology. The 3d metal is in the center and the 4f in the wings, as shown in the cartoon representation (Figure 1). In accord with our previous findings, the 3d and 4f metals are separated by 3.3±0.1 Å. Five out of six and six out of eight coordination sites of the 3d and 4f centers respectively are occupied by the ligand.

Thermal Studies. Thermogravimetric analysis for compounds **2ZnY-21ZnY** (see ESI Figures S26-S45) display similar behavior. As the temperature in increased, the mass of the CCs decreases slowly up to 280-320°C. This decrease is between 6-13% depending on overall molecule weight and corresponds to the loss of the two solvent DMF molecules. Once this temperature is exceeded, the mass rapidly decreases up to 400°C, which is indicative of decomposition. This decrease becomes less significant and plateaus after 600°C and with all examples the remaining mass is constant by 800°C. The residual % mass is between 19-25% depending on initial molecular mass and corresponds to the remaining metal oxides (ZnO/Y_2O_3, 2:1).

Catalytic experiments. Our initial benchmarking studies leading up to the synthesis of the above library of **ZnY** CCs, examined the reaction of 1,3-dimethyl barbituric acid with *trans*-β-nitrostyrene in ethanol. This reaction proceeds only slowly in the absence of a catalyst (*i.e.* 35% conversion in 1 h). Zn salts alone do not promote the transformation but some lanthanide salts give moderate yields (see SI, Table S3). Using a range of our previously reported 3d/4f CCs as catalysts at a 2.5 mol% loading level, **1ZnSm, 1ZnEu, 1ZnTb, 1ZnGd, and 1ZnDy** were found to give moderate performance but the use of **1ZnY** and **1ZnYb** provided the MA product in quantitative yield within 15 minutes at room temperature (see SI, Table S4). Taking into account the relative prices of Y and Yb, we selected to evaluate the performance of **1ZnY** further. After screening several solvents, we identified that the ethanol/water (6:4) solvent system was optimal in terms of rate and is also advantageous from an environmental impact[35] perspective (Table S5). Then, we confirmed that reaction at room temperature rather than at -5°C or reflux gave the highest yields (Table S6) and that loadings of 2.5 mol% rather than 5 or 10 mol% gave highest yields (Table S7). Using these optimized conditions, we then explored the scope of the reaction using an array of substituted nitrostyrenes (Table 2). Compounds **I-V** and **VII** have been reported previously.[31] We were now in a position to evaluate the performance of our library of CCs containing the different ligands: **2ZnY-21ZnY** (Table S8). The results indicated the superiority of catalyst **17ZnY** which was found to give excellent yields even when using a loading level of just 0.5 mol% (Tables S9 and S10). The ligand in

this CC contains the allyl and *bis*-(4-*tert*-butyl-2-aminophenol) substructure which we hypothesize may provide improved solubility relative to the other ligands.
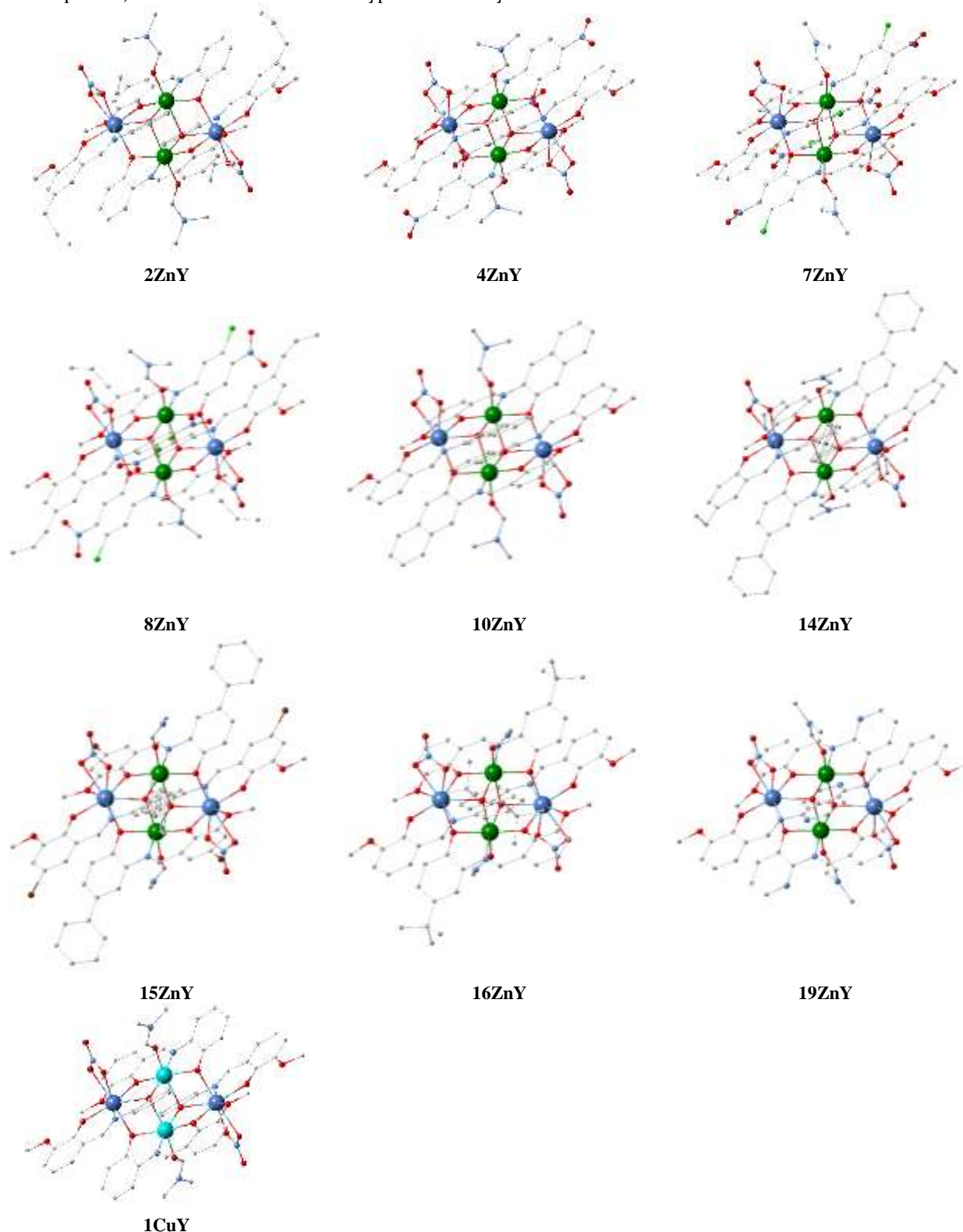
Figure 2. The crystal structures of **2ZnY, 4ZnY, 7ZnY, 8ZnY, 10ZnY, 14ZnY, 15ZnY, 16ZnY, 19ZnY** and **1CuY**. Colour code; Zn, green; Y, mauve; Cu, light blue; O, red; N, blue; C, grey; Cl, light green; Br, brown.

In general, all these reactions give the products in very good to quantitative yields. The structures of compounds **VI**, **VIII** and **XII** were confirmed by single crystal X-ray structure determination (see SI, Figure S1).

Mechanistic studies. In order to gain information about the possible mechanism of this reaction and to delineate the scope and limitations of the **17ZnY** catalyst, we performed the following set of reactions.

Table 2 The scope of reactions of 1,3-dimethyl barbituric acid and derivatives with *trans*-β-nitrostyrenes catalyzed by **1ZnY**.

Product	Substitution		Yield[a]	Time
	I. $R_2 = C_6H_5$,	$R_3 = H$,	Quantitative,	15min
	II. $R_2 = p\text{-}CH_3OC_6H_4$,	$R_3 = H$,	75%,	15min
	III. $R_2 = p\text{-}CH_3C_6H_4$,	$R_3 = H$,	99%,	15min
	IV. $R_2 = p\text{-}FC_6H_4$,	$R_3 = H$,	99%,	15min
	V. $R_2 = p\text{-}BrC_6H_4$,	$R_3 = H$,	99%,	15min
	VI. $R_2 = C_6H_5$,	$R_3 = CH_3$,	94%,	15min
	VII. $R_2 = C_4H_4O$,	$R_3 = H$,	Quantitative,	15min
	VIII. $R_2 = C_6H_5$,	$R_3 = H$,	Quantitative,	15min
	IX. $R_2 = p\text{-}CH_3OC_6H_4$,	$R_3 = H$,	95%,	20min
	X. $R_2 = p\text{-}CH_3C_6H_4$,	$R_3 = H$,	80%,	20min
	XI. $R_2 = p\text{-}FC_6H_4$	$R_3 = H$,	Quantitative,	20min
	XII. $R_2 = p\text{-}BrC_6H_4$,	$R_3 = H$,	96%,	20min
	XIII. $R_2 = C_6H_5$,	$R_3 = CH_3$,	81%,	15min
	XIV. $R_2 = C_4H_4O$,	$R_3 = H$,	96%,	15min
	XV. $R_2 = C_6H_5$,	$R_3 = H$,	81%,	60min
	XVI. $R_2 = p\text{-}CH_3OC_6H_4$,	$R_3 = H$,	80%,	60min
	XVII. $R_2 = p\text{-}CH_3C_6H_4$,	$R_3 = H$,	76%,	60min
	XVIII. $R_2 = p\text{-}FC_6H_4$	$R_3 = H$,	79%,	60min
	XIX. $R_2 = p\text{-}BrC_6H_4$,	$R_3 = H$,	80%,	60min
	XX. $R_2 = C_6H_5$,	$R_3 = CH_3$,	78%,	60min
	XXI. $R_2 = C_4H_4O$,	$R_3 = H$,	79%,	60min

[a] Isolated

Influence of bases: Two reactions were performed in the presence of base (Et_3N or NaOH), however a significant lowering of the catalytic conversion was observed. This outcome can likely be attributed to the instability of the CC in the presence of base which can effect conversion to other CCs (Table S11).

Tuning the 3d metal: To further understand the role of the metals in **17ZnY**, we performed parallel reactions using the isoskeletal compounds **1NiDy**,[36,37] **1CoDy**[36,37] and **1CuY** (see SI). The reactions of **1CuDy** and **1ZnDy** yielded the desired product in very good yields (90%) while with **1NiDy** and **1CoDy** had poor performance (Table 3). These differences can be rationalized taking into account the Irving-Williams[38] stability series, in which for a given ligand the stability of dipositive metal ion complexes increases in the order: $Co^{II} < Ni^{II} < Cu^{II} < Zn^{II}$. It would therefore appear that binding (*i.e.* activation) of at least one of the substrates *via* an O atom to a 3d metal center is required for efficient catalysis.

NMR studies: Careful titration of DMF solutions of **1ZnY** with 0.25-10 eq. of *trans*-β-nitrostyrene or of 6-amino-1,3-dimethyluracil lead to no significant observable changes in the ¹H NMR spectra. On the other hand, analogous titrations with *N,N'*-diethyl-2-thiobarbituric acid led to significant differences: both the *N,N'*-diethyl-2-thiobarbituric acid and **1ZnY** peaks were affected. Evidently binding of the individual substrates to the **1ZnY** is not strong, but this presents no impediment to the catalytic activity of the complex.

UV Vis studies: The reaction of *trans*-β-nitrostyrene (1×10⁻⁵ mmol) and dimethylbarbituric acid (1×10⁻⁵ mmol) in the presence of **1ZnY** was investigated by UV-Vis spectroscopy in a water/ethanol solution (see SI, Figure S2). The *trans*-β-nitrostyrene exhibits a strong absorption at 320 nm. The absorption was recorded over 70 min with 5 min intervals between measurements. It was observed that the intensity of the peak at 320 nm gradually decreased and the intensity of the product (347 nm) gradually increased. The reaction proceeds much slower in absence of catalyst, demonstrating the need for catalyst (see SI, Figure S3). *trans*-β-Nitrostyrene and dimethylbarbituric acid were also left for 60 min to react before 2.5% mmol of **1ZnY** was added; the reaction proceed faster in the presence of the catalyst (see SI, Figure S4).

Table 3. Comparison of efficacy for compounds **1ZnY**, **1ZnDy**, **1NiDy**, **1CoDy** and **1CuDy**.

Entry	Loading/%	Catalyst	Yield/%	Time /min
1	2.5	**1ZnY**	quantitative	15
2	2.5	**1ZnDy**	94	15
3	2.5	**1NiDy**	29	15
4	2.5	**1CoDy**	34	15
5	2.5	**1CuDy**	85	15

EPR studies: To gain further mechanistic insights, the following Q-band EPR studies of **1ZnGd** in solution at 15K were performed. *trans*-β-Nitrostyrene or 1,3-dimethyl barbituric acid, dissolved in EtOH, was added to ethanolic solutions of **1ZnGd** (1:1, 20:1 and 40:1 ratios). Additionally, a mixture of *trans*-β-nitrostyrene and 1,3-dimethyl barbituric acid, dissolved in EtOH (1:1 ratio), was added to ethanolic solutions of **1ZnGd** (1:1, 20:1 and 40:1 ratios) (see SI, Figure S5). The experiments in ratios 20:1 and 40:1 were executed to mimic the catalytic conversion (100:5 and 100:2.5) conditions and identify the stability of the bimetallic system.

Numerical spectrum simulations of the EPR spectra of the 3d/4f CCs were performed. The conventional forms of spin Hamiltonians, i.e. $\hat{H}_{spin} = \mathbf{S} \cdot \mathbf{D} \cdot \mathbf{S} + \beta_e \mathbf{B_o} \cdot \mathbf{g} \cdot \mathbf{S}$, were considered where the first term denotes the fine-structure splitting (zero-field splitting - ZFS), and the second term denotes the electron Zeeman interaction. For the S-state $4f^7$ (Gd^{3+}) ions, they usually exhibit an orbital singlet ground state and the degeneracy $2J + 1$ of each S multiplet can be partially or wholly lifted. Regarding the complex nature of the observed experimental spectra, the spin-orbit coupling (SOC) must have a significant orbital contribution to the low-lying spin ground state. There is likely a competing effect between the ZFS energy of $S = 7/2$ state and the crystal-field energy of Gd^{3+} ($4f^7$), including Zn^{2+} ($3d^{10}$), even though the latter is diamagnetic. The EasySpin computational simulation package[39] was used to allow a reasonable parameter set for D-values and effective g'-factors to be obtained.

Only the permissible transitions ($\Delta m_S = \pm 1$) between the electron spin $m_S = \pm 1/2$ and $m_S = \pm 3/2$ sublevels of Gd^{3+} were expected to be observed at X-band microwave frequency whose excitation energy is obviously not enough to resolve the transitions between high-spin multiplets. All the EPR spectra were broadened significantly at 340 mT while there was a sharp transition at 1200 mT. Since, in orientation disordered powder-type samples (including frozen solutions), paramagnetic species are randomly oriented with respect to the applied magnetic field B_o, and their EPR spectra appear as the sum of the resonances of all those orientations. In such conditions, the powder-type spectra provide only limited information on the orientation of the **g**-tensor principal axes in the molecular coordinate system (see SI, Figure S6).

Table 4. Spin Hamiltonian parameters obtained from EasySpin numerical simulations.

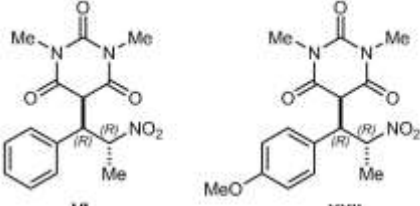| Samples	Effective g-factors			$\vert D \vert$ [MHZ]	HWHM [MHz]
	g'_1	g'_2	g'_3		
1ZnGd with BA (1:1)	1.961	0.563	0.563	158(30)	36
1ZnGd with NS (1:1)	1.961	0.563	0.560	128(20)	32
1ZnGd with BA and NS (1:1)	1.951	0.570	0.560	108(10)	46
1ZnGd with BA (1:20)	1.951	0.570	0.560	108(10)	46
1ZnGd with NS (1:20)	1.961	0.572	0.552	96(10)	33
1ZnGd with BA and NS (1:20)	1.951	0.570	0.560	108(10)	46
1ZnGd with BA (1:40)	1.951	0.570	0.560	108(10)	46
1ZnGd with NS (1:40)	1.961	0.570	0.560	96(10)	40
1ZnGd with BA and NS (1:40)	1.951	0.570	0.560	108(10)	46

We were able to assign the electronic splitting to the partially resolved transitions at 340 and 1200 mT. The corresponding energy levels were obviously not well-separated, indicating that m_S could not become the main quantum numbers. Thus, fictitious spin states are likely responsible for the observed splitting separated at $g'_\parallel$ and $g'_\perp$ regions. The numerically simulated spectra produced rather good agreements with the experimental ones (see SI, Figure S7), and their corresponding parameters are given in Table 4. These are likely not the only parameter sets, and the further refinements can probably be achieved. Importantly, the slight differences in g-factors are taken as evidence in support of the Gd coordination environment changes, particularly in the $g'_\perp$ region. We believe that the coordination number remains intact since the overall molecular symmetry is unambiguously reflected on the experimental g-tensor. On the other hand, the existence of the large ZFS ($h\nu \ll D$) can be tested using a series of high-order electron spin operators in the spin Hamiltonians, including the extended Stevens operators.[40] We attempted such simulations to obtain a plausible parameter set, but the simulated spectra did not reproduce reasonable matches with the experiments (spectra not shown). Only transitions within the ground Kramers doublet of the $J = 7/2$ ground term of Gd^{3+} ($^8S_{7/2}$) are observed as a fictitious (or effective) spin $S' = 1/2$ system at X-band, with the ground state g-factors of $g'_\parallel \sim 1.961$ and $g'_\perp \sim 0.561$, regarding the unknown rhombicity of ZFS and the ratio between SOC and crystal-field energy.

The effects of the hyperfine fields created by ^{155}Gd and ^{157}Gd (both $I = 3/2$) nuclei on the alignment of the electron spins are negligible, and the electron problem can be treated independently. ^{67}Zn ($I = 5/2$) nucleus has only a contribution to inhomogeneous line broadenings. In addition, hyperfine interaction of ligands is overwhelmed and readily masked by such broadening effects.

Test of diastereoselectivity: When we employed *trans*-β-methyl-nitrostyrene instead of *trans*-β-nitrostyrene in the reaction with 1,3-dimethyl barbituric catalyzed by 1ZnY (2.5 mol%), excellent yields of product **VI** were obtained within 15 min (Table 2). The NMR data showed the presence of one diastereoisomer (> 20:1 *dr*) (see SI). A single crystal X-ray structure determination on this product obtained after filtration of the reaction in the presence of the catalyst, revealed this to have the (*R*,R**) relative configuration. Next, we explored the influence of the lanthanide on the diastereoselectivity of this reaction (Table 5). We ran parallel reactions using 1ZnSm, 1ZnEu, 1ZnGd, 1ZnDy, 1ZnTb and 1ZnYb as catalysts under otherwise identical conditions (Entries 1-7). Only slight differences in diastereoselectivy were observed (20:1 for 1ZnY to >20:1 for 1ZnSm) which might be attributed to the different ionic radii of the Lanthanides. Subsequently, we investigated 1CoY, 1NiY and 1CuY as catalysts and observed that all three CCs gave ~20:1 *dr*s, but that 1CoY and 1NiY gave significantly lower yields (Entries 8-10). We also performed the reaction of *cis*-β-methyl-4-methoxy-nitrostyrene with 1,3-dimethyl barbituric acid with 1ZnY as catalyst to yield product **XXII** (Table 4). The NMR data again showed the presence of one diastereoisomer, which X-Ray characterization revealed also to have the (*R*,R**) relative stereochemistry (Figure S2). Use of 1ZnSm, 1ZnEu, 1ZnGd, 1ZnDy, 1ZnTb, 1ZnYb, 1CoY, 1NiY and 1CuY as catalysts gave similar *dr*s and yields to those with *trans*-β-methyl-nitrostyrene (Entries 2-10).

Table 5. Comparison of efficacy for compounds 1ZnY, 1ZnDy, 1NiDy, 1CoDy and 1CuDy.

| Entry	Catalyst	VI	XXII
		Yield (%) /dr[a] (R*,R*/R*,S*)	Yield (%) /dr[a] (R*,R*/R*,S*)
1	1ZnY	quantitative / 20:1	96 / 20:1
2	1ZnSm	75 / >20:1	69 / >20:1
3	1ZnEu	81 / >20:1	74 / >20:1
4	1ZnGd	89 / >20:1	77 / >20:1
5	1ZnDy	94 / >20:1	89 / >20:1
6	1ZnTb	88 / >20:1	85 / >20:1
7	1ZnYb	quantitative / 20:1	93 / 20:1
8	1CoY	24 / 20:1	41 / 20:1
9	1NiY	19 / 20:1	30 / 20:1
10	1CuY	71 / 20:1	94 / 20:1

[a]dr = diastereoisomeric ratio

Computational studies: To gain insight into a plausible mechanism of the MA of 1,3-dimethyl barbituric acid to *trans*-β-nitrostyrenes catalyzed by 3d/4f CCs we performed a series of calculations on possible reaction pathways employing density functional theory (DFT) methods and monitoring the natural atomic charge distribution and the nature of the frontier molecular orbitals (FMOs) on both the catalyst and the substrates. Computational details with the relevant citations are given in the SI. We selected to examine 1,3-dimethyl barbituric acid and 6-amino-1,3-dimethyl barbituric acid with (Z)-(2-nitrovinyl)benzene, (Z)-(2-nitroprop-1-enyl)benzene and (Z)-1-methoxy-4-(2-nitroprop-1-enyl)benzene. To avoid any confusion when discussing the mechanistic details of the MA reaction catalyzed by the ZnY bimetallic catalyst, the chemical structures of the selected molecules with a labeling scheme are shown in Figure 3. Firstly, we calculated the thermodynamics of the non-catalyzed MA reactions in aqueous solution employing the PBE0/6-311++G(d,p) computational protocol to obtain natural atomic charges calculated by Natural Bond Orbital (NBO) population analysis. The relevant FMOs are shown in Figure S7.

It is well established that the α-carbon of barbituric acid has a reactive hydrogen atom and is quite acidic (pK$_a$ = 4.01) because of the aromatic stabilization of the carbanion. DFT calculations at the PBE0/6-311++G(d,p) level of theory revealed that the keto form of 1,3-dimethyl barbituric acid in aqueous solution can co-exist in equilibrium with the diketo-enol form, which is found at 8.7 kcal/mol higher in energy than the triketo form (Figure 3). Notice that *ab initio* and DFT calculations on the tautomers of barbituric acid showed that the triketo form is found to be the most stable form in the gas phase and in solution, which is in agreement with the experimental result.[41–45] On the other hand, the aminodiketo form of 6-amino-1,3-dimethyl barbituric acid is the most stable form relative to the aminoketo-enol and diketo-ammonium forms, which are found 47.0 and 63.6 kcal/mol higher in energy. According to NBO population analysis the keto and enolic oxygen atoms of the diketo-enolic tautomer acquire higher negative natural atomic charges by 0.03 up to 0.06 |e|

relative to the corresponding oxygen atoms of the triketo tautomer. On the other hand, the α-carbon atom in the enolic tautomer acquires less negative natural atomic charge by 0.114 |e| relative to the α-carbon atom of the triketo tautomer. In the 6-amino 1,3-dimethyl barbiturate substrate the keto oxygen atoms acquire higher negative natural atomic charges by 0.055 up to 0.080 |e| relative to the corresponding oxygen atoms of the triketo tautomer of the 1,3-dimethyl barbiturate substrate, while the α-carbon atom acquires less negative natural atomic charge by 0.12 |e|.

The highest occupied molecular orbital (HOMO) in the triketo tautomer is mainly localized on the keto-oxygen atoms adjacent to the α-carbon atom (64.4% having 2p character), while in the diketo-enolic tautomer is mainly localized on the α-carbon atom (44.6% having 2p character) and the adjacent keto-oxygen atom (13.5% with 2p character). Both the nature of the HOMOs and the negative charge distribution suggest that the triketo form of the 1,3-dimethyl barbiturato ligand could be coordinated to a metal center through the keto-oxygen donor atoms, while the diketo-enolic form through the α-carbon atom. Similarly, the nature of HOMO of the 6-amino-1,3-dimethyl barbiturate substrate supports coordination through the α-carbon atom.
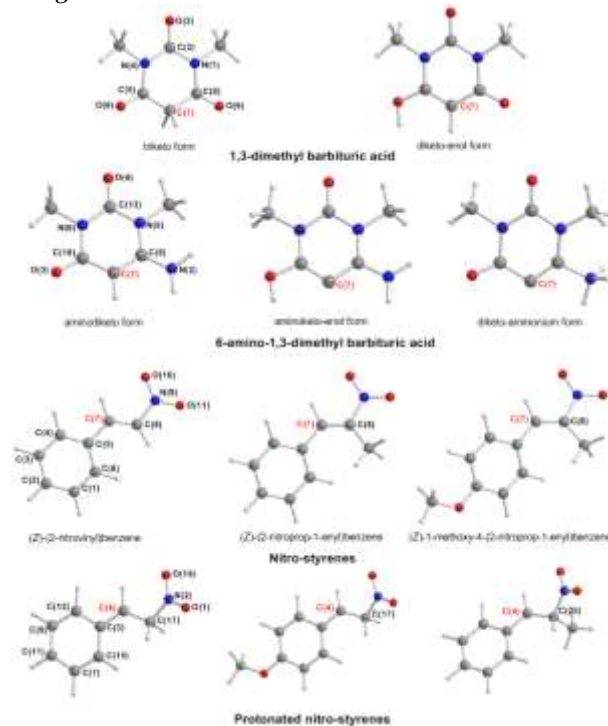
Figure 3. Natural atomic charges and the relevant FMOs of the triketo and diketo-enol forms of 1,3-dimethyl barbituric acid, the aminodiketo, aminoketo-enol and diketo-ammonium forms of 6-amino 1,3-dimethyl barbituric acid and the (Z)-(2-nitrovinyl)benzene, (Z)-(2-nitroprop-1-enyl)benzene and (Z)-1-methoxy-4-(2-nitroprop-1-enyl)benzene calculated at the PBE0/6-311++G(d,p) level of theory in aqueous solutions. The C(7) labels on nitrostyrenes are in bold.

The non-catalyzed MA reactions of the triketo tautomer of 1,3-dimethyl barbituric acid to (Z)-(2-nitrovinyl)benzene, (Z)-(2-nitroprop-1-enyl)benzene and (Z)-1-methoxy-4-(2-nitroprop-1-enyl)benzene are predicted to be exothermic by 11.9, 9.9 and 10.9 kcal/mol respectively, while the exothermicity of the addition of the diketo-enol tautomer of 1,3-dimethyl barbituric acid to (Z)-(2-nitrovinyl)benzene, (Z)-(2-nitroprop-1-enyl)benzene and (Z)-1-methoxy-4-(2-nitroprop-1-enyl)benzene are 20.7, 18.6 and 19.6 kcal/mol respectively at the PBE0/6-311++G(d,p) level of theory. The non-catalyzed MA reactions of the 6-amino-1,3-dimethyl bar-

biturate substrate to (Z)-(2-nitrovinyl)benzene, is predicted to be also exothermic by 13.2 kcal/mol. Considering the nature of the lowest unoccupied molecular orbital (LUMO) of the (Z)-(2-nitrovinyl)benzene, (Z)-(2-nitroprop-1-enyl)benzene and (Z)-1-methoxy-4-(2-nitroprop-1-enyl)benzene being a π^* MO mainly localized on the NO$_2$ moiety (51.2%, 57.5% and 56.9%) and on the C(7) unsaturated carbon atom (22.8%, 21.4% and 21.8%), the MA reactions under study are FMO-controlled supported by HOMO-LUMO interactions.
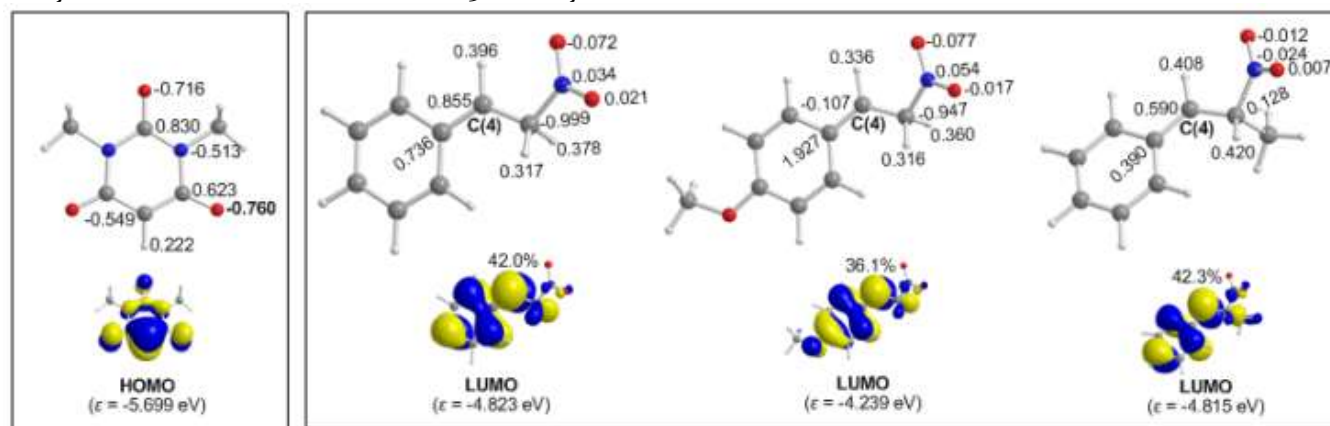
Figure 4. Natural atomic charges and relevant FMOs of the 1,3-dimethyl barbiturate carbanion and the protonated (Z)-(2-nitrovinyl)benzene, (Z)-1-methoxy-4-(2-nitrovinyl)benzene and (Z)-(2-nitroprop-1-enyl)benzene calculated at the PBE0/6-311++G(d,p) level of theory in aqueous solutions. The C(4) labels on the protonated nitro-styrenes are in bold.

An alternative plausible reaction pathway involves the nucleophilic attack of the **C(4)** electrophilic center of the protonated *trans*-β-nitrostyrenes, namely (Z)-(2-nitrovinyl)benzene, (Z)-(2-nitroprop-1-enyl)benzene and (Z)-1-methoxy-4-(2-nitroprop-1-enyl)benzene and by the nucleophilile 1,3-dimethyl barbiturate carbanion (Figure 4).

The deprotonation of the triketo form of 1,3-dimethyl barbituric acid to form the 1,3-dimethyl barbiturate carbanion is predicted to be endothermic by 45.1 kcal/mol. Of note is a remarkable increase in the negative atomic charge of the keto oxygen atoms in the carbanion relative to the corresponding keto oxygen atoms of the triketo tautomer. On the other hand the negative natural atomic charge on the deprotonated α-carbon atom of the carbanion decreases by 0.04|e|. Interestingly, the HOMO of the nucleophile is primarily localized on the deprotonated α-carbon atom (52.3%) and the two adjacent keto oxygen atoms (28.9%) being π^*-type MOs, while the LUMOs of the protonated (Z)-(2-nitrovinyl)benzene, (Z)-(2-nitroprop-1-enyl)benzene and (Z)-1-methoxy-4-(2-nitrovinyl)benzene are mainly localized on the electrophilic C(2) carbon atom (42.0%; 36.1% and 42.3% respectively) (Figure 5). It is apparent that the nucleophilic attack at the electrophilic C(2) carbon atom by the carbanion is a FMO-controlled process supported by the interaction of the HOMO(nucleophile) with the LUMO(electrophile). The nucleophilic attack at the electrophilic C(2) carbon atom of the protonated (Z)-(2-

nitrovinyl)benzene, (Z)-(2-nitroprop-1-enyl)benzene and (Z)-1-methoxy-4-(2-nitrovinyl)benzene by the 1,3-dimethyl barbiturate carbanion are predicted to be strongly exothermic by 61.4, 58.7 and 49.1 kcal/mol respectively.

To probe the electrophilic/nucleophilic character of the *trans*-β-nitrostyrene molecules, selected electronic descriptors (condensed Fukui function, fC(7),[46,47] condensed dual descriptor ΔfC(7),[48] proton affinity, *PA* and chemical potential, μ[49,50]) were calculated by the PBE0/6-311++G(d,p)/PCM computational protocol in order to find out how the electrophilic/nucleophilic character of the electrophilic/nucleophilic centers of the *trans*-β-nitrostyrenes affect the efficacy of the MA reaction (see SI, Table S12).

The Fukui function, which is an important concept in conceptual DFT, has been widely used in prediction of reactive site of molecules. The Fukui function is defined as:

$$f(\mathbf{r}) = \left[\frac{\partial \rho(\mathbf{r})}{\partial N}\right]_v$$

where *N* is number of electrons in present system. The constant term *v* in the partial derivative is the external potential. In the finite difference approximation, the Fukui function can be calculated unambiguously for three situations:

Nucleophilic attack: $f^+(\mathbf{r}) = \rho_{N+1}(\mathbf{r}) - \rho_N(\mathbf{r}) \sim \rho^{LUMO}(\mathbf{r})$
Electrophilic attack: $f^-(\mathbf{r}) = \rho_N(\mathbf{r}) - \rho_{N-1}(\mathbf{r}) \sim \rho^{HOMO}(\mathbf{r})$

The dual descriptor is another useful function used to reveal reactive sites. Formally, the definition of the dual descriptor Δf has close relationship with the Fukui function:

$$\Delta f(\mathbf{r}) = f^+(\mathbf{r}) - f^-(\mathbf{r})$$

$\Delta f(\mathbf{r})$ predicts both types of reactive sites simultaneously. It is argued that when $\Delta f > 0$, the site is favorable to nucleophilic attack, whereas when $\Delta f < 0$, the site is favorable for electrophilic attack.
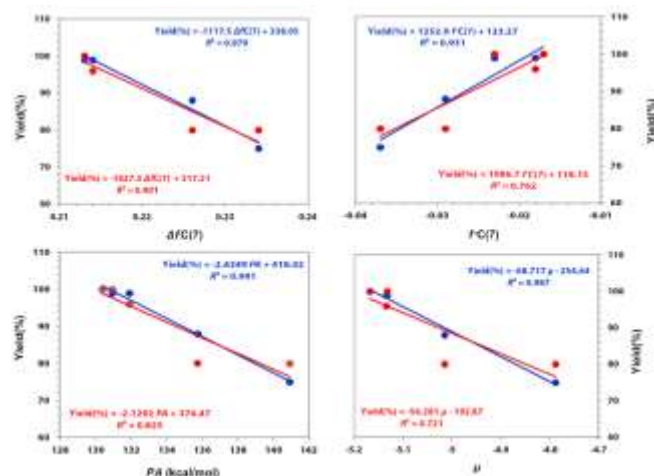
Figure 5. Linear relationships between Yield(%) *vs.* ΔfC(7), Yield(%) *vs.* fC(7), Yield(%) *vs.* PA and Yield(%) *vs.* μ correlations calculated at the PBE0/6-311++G(d,p) level of theory in aqueous solutions.

Excellent linear relationships are obtained for the Yield(%) *vs.* ΔfC(7) and Yield(%) *vs.* fC(7) correlations. Good linear relationships are also obtained for the Yield(%) *vs.* PA and Yield(%) *vs.* μ correlations ($\mu = (\varepsilon_{HOMO} + \varepsilon_{LUMO})/2$) (Figure 5).

These correlations show that the nucleophillic character of the C(7) carbon atom of the *trans*-β-nitrostyrenes affects the efficacy of the MA reaction. Upon protonation the C(2) carbon atom in the protonated *trans*-β-nitrostyrenes becomes an electrophilic center. The calculated electronic descriptors related with the electrophilic character of the C(2) carbon atom in the protonated *trans*-β-nitrostyrene molecules are given in the SI (Table S13). Excellent linear relationships are obtained for the Yield(%) *vs.* fC(2) and Yield(%) *vs.* QC(2) correlations (f^+C(2) is the condensed Fukui function for electrophilic attack) (Figure 6). However, poor linear relationship is obtained for the Yield(%) *vs.* fC(2) correlation, since the C(2) carbon atom in the protonated *trans*-β-nitrostyrene molecules is not susceptible to electrophilic attack.
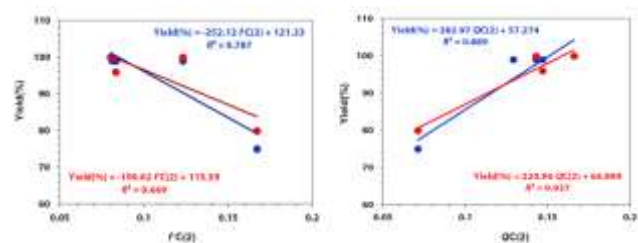
Figure 6. Linear relationships between Yield(%) *vs.* fC(2) and Yield(%) vs QC(2) correlations calculated at the PBE0/6-311++G(d,p) level of theory in aqueous solutions.

The above correlations show that the electrophilic character of the C(2) carbon atom would affect the efficacy of the MA reaction, since it determines the strength of the nucleophilic attack by the 1,3-dimethyl barbiturate carbanion nucleophile. In summary, the MA reaction should involve first a proton transfer from the 1,3-dimethyl barbituric acid to the **C**(NO$_2$)Me carbon atom, which is accompanied by charge density redistribution rendering the C(2) carbon atom electrophilic center that is attacked by the nucleophile 1,3-dimethyl barbiturate carbonation formed.

To gain insights into the activation of the substrates of the MA reaction catalyzed by the bimetallic ZnY catalysts we explored all possible coordination modes of the substrates to the metal centers of the catalysts by means of DFT calculations at the PBE0/Def2-TZVP(Zn,Y)∪6-31G(d,p)(E) (E = main group element) level of theory in aqueous solution using a representative catalyst, **7ZnY**. The estimated binding energy of nitrate to the Y metal center is 30.8 kcal/mol. Therefore dissociation of the nitrate seems to be difficult. However, examination of the defect dicubane structure of the catalyst suggests that its dissociation into dinuclear species in solution may well be possible. It can be seen that the two dimeric species in the defect dicubane structure are loosely associated, for the Zn-O distances of 2.430 and 2.398 are longer than the Zn-O distances of 2.085 and 2.059 of the loosely associated DMF with Zn (Figure 7). Compare also with the Zn-O distances of 2.037 and 2.052 between Zn and the bridging O atom. Similarly the Y-O distances are very long and indicative of weak interactions.
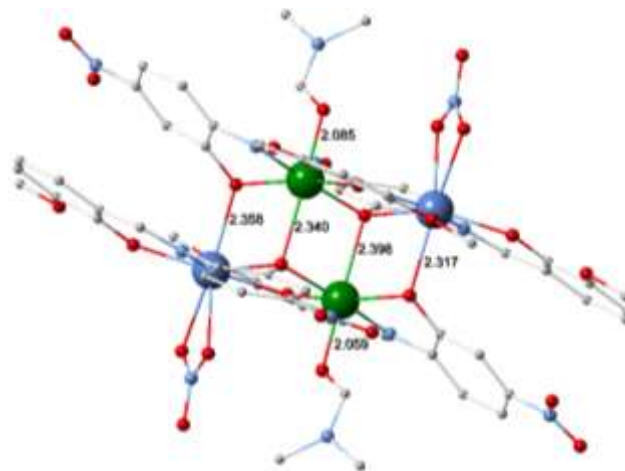
Figure 7. The defect dicubane structure of the catalyst with the estimated intermolecular Y⋯O and Zn⋯O distances between the dinuclear species indicative of a loose association of the dimers in the defect dicubane structure. Color code; Zn, green; Y, mauve; O, red; N, blue; C, grey;

Then, we calculated the natural atomic charges on the metal centers of the **ZnY** bimetallic catalysts which have

been characterized crystallographically using their crystal structures in aqueous solution and analyzed the MOs for only the representative catalyst **7ZnY**. The natural atomic charges along with the efficacy for these catalysts are compiled in Table 6, while the 3D plots of FMOs of the representative catalyst **7ZnY** are shown in the SI (Figure S8).

Inspection of the FMOs of **7ZnY** catalyst reveals that the virtual acceptor FMOs (LUMO, LUMO+1, LUMO+2, LUMO+3, etc) are of π^*-type located on the ligands. As no acceptor orbital is located on the metal centers of the ZnY bimetallic catalyst coordination of the MA substrates to the metal centers supported by the interaction of the acceptor orbitals with the donor orbitals (HOMO, HOMO-1, HOMO-2, *etc*.) of the substrates is not feasible. Therefore, the substrates interact with the bimetallic catalyst through non covalent interactions (electrostatic and dispersion forces). All attempts to optimize the geometry of the **7ZnY**-barbiturate substrate adducts, with the barbiturate substrate approaching the Y metal center were failed. In contrast, a local minimum was located on the potential energy surface (PES) of a **7ZnY**-barbiturate adduct involving coordination of barbiturate to Zn metal atom of the catalyst upon dissociation of the coordinated DMF ligand. Note that the estimated binding energy of DMF to Zn metal center is 10.7 kcal/mol at the PBE0/Def2-TZVP(Zn,Y)$\cup$6-31G(d,p)(E) (E = main group element) level of theory in aqueous solutions. The binding of the barbiturate substrate to Zn metal center is very weak, the estimated binding energy found to be 2.8 kcal/mol, which is indicative of weak non covalent interactions. The calculated distance between the Zn and the keto O atom of the triketo form of the 1,3-dimethyl barbituric acid was found to be 2.140 Å. On the other hand, *trans*-β-nitrostyrene substrates showed a preference to be coordinated to Y metal center of the **7ZnY** catalyst, *via* a unidentate coordination mode,[51] the estimated binding energy predicted to be 4.3 kcal/mol at the PBE0/Def2-TZVP(Zn,Y)$\cup$6-31G(d,p)(E) (E = main group element) level of theory in aqueous solutions. The calculated distance between the Y and the O atom of the unidentate *trans*-β-nitrostyrene substrate was found to be 2.445 Å. On approaching the *trans*-β-nitrostyrene substrate to Zn central atom resulted in a local minimum corresponding to a very weak association of the barbiturate substrate with the **7ZnY** catalyst, but the binding energy is marginal (0.2 kcal/mol). Then we optimized the geometry of the adduct formed upon interaction of the *trans*-β-nitrostyrene substrate with the Y metal center of the **7ZnY**-barbiturate adduct. In this adduct the barbiturate and *trans*-β-nitrostyrene substrates are both coordinated to the Zn and Y metal centers of the **7ZnY**-catalyst respectively. The estimated Zn-O and Y-O bond distances are predicted to be 2.135 and 2.454 Å respectively. For this adduct the estimated binding energy of the *trans*-β-nitrostyrene-Yttrium interaction is 4.1 kcal/mol. The equilibrium geometries of the **7ZnY**-barbiturate and **7ZnY**-*trans*-β-nitrostyrene adducts optimized at the PBE0/Def2-TZVP(Zn,Y)$\cup$6-31G(d,p)(E) (E =

main group element) level of theory in aqueous solutions are given in the SI (Figure S9).

Table 6. Natural atomic charges on the metal centers of 3d/4f ZnY bimetallic catalyst calculated at the PBE0/Def2-TZVP(Zn,Y)$\cup$6-31G(d,p)(E) (E = main group element) level of theory in aqueous solutions.

| Catalyst	Yield (%)	Q_{Zn}	Q_Y
2ZnY	100	1.308	1.935
16ZnY	100	1.311	1.929
19ZnY	98	1.326	1.942
10ZnY	86	1.320	1.945
14ZnY	86	1.325	1.932
8ZnY	73	1.322	1.937
7ZnY	55	1.330	1.927
4ZnY	43	1.331	1.926
15ZnY	42	1.307	1.935

It can be concluded that that the barbiturate and *trans*-β-nitrostyrene substrates for the MA reaction catalyzed by the ZnY bimetallic catalyst are cooperatively activated through their interaction with the Zn and Y metal centers of the catalyst following the proposed mechanism shown in Scheme 1.
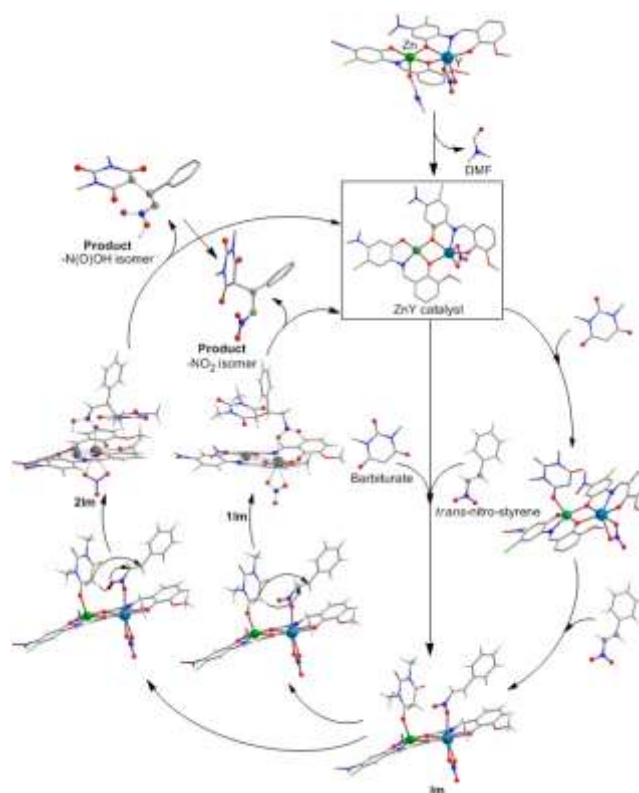
Scheme 1. A proposed mechanism involving the cooperative activation of both the barbiturate and *trans*-β-nitrostyrene substrates *via* their coordination to the Zn and Y metal centers of the ZnY catalyst.

In the proposed mechanism, initially the barbiturate substrate is coordinated to the Zn metal center of the **7ZnY** catalyst after dissociation of the coordinated DMF solvent molecule and then coordination of the *trans*-β-

nitrostyrene substrate to the Y metal center of the catalyst. This could be a stepwise process or both substrates could be simultaneously coordinated to the metal centers of the catalyst yielding the intermediate **Im**. The coordination of the substrates to the Zn and Y metal centers yielding **Im** is a slightly exothermic process, the estimated exothermicity is predicted to be 6.9 kcal/mol at the PBE0/Def2-TZVP(Zn,Y) $\cup$ 6-31G(d,p)(E) (E = main group element) level of theory. The two substrates upon coordination to the metal centers are brought into proximity such that a proton can be transferred from the α-carbon atom of the barbiturate to the **C**H(NO$_2$) carbon atom of the coordinated *trans*-β-nitrostyrene followed by the nucleophilic attack of the resulting barbiturate carbanion to the electrophilic **C**(7) carbon atom of the *trans*-β-nitrostyrene to yield the intermediate **1Im**. These processes are shown by the arrows drawn on the relevant **Im** structures of the catalytic cycle (Scheme 1). This intermediate comprises the MA product weakly bound to the Y metal center through the O donor atom of the NO$_2$ moiety (Figure 8). The formation of this intermediate is a slightly exothermic process, the estimated exothermicity being 6.4 kcal/mol. The coordinated product in **1Im** immediately dissociates yielding the catalyst with release of 1.0 kcal/mol. Alternatively the proton could be transferred from the α-carbon atom of the barbiturate substrate to the uncoordinated O atom of the NO$_2$ moiety of the *trans*-β-nitrostyrene, resulting in transformation of the NO$_2$ group into an N(O)O**H** group, followed by the nucleophilic attack of the barbiturate carbanion on the electrophilic **C**(7) carbon atom of the *trans*-β-nitrostyrene yielding the intermediate **2Im**. The proton transfer and the nucleophilic attack processes are shown by the arrows drawn on the relevant **Im** structures of the catalytic cycle (Scheme 1). The MA product would then be weakly associated with the Y metal center through the uncoordinated O donor atom of the N(O)O**H** moiety (Figure 8). The formation of this isomeric intermediate is also a slightly exothermic process, the estimated exothermicity being 4.8 kcal/mol. The dissociation energy for the release of the –N(O)OH product is 13.9 kcal/mol and this released product readily isomerizes to the more stable (by 16.6 kcal/mol) -NO$_2$ product. Comparison of the two possible reaction pathways reveals that the first pathway involving the formation of **1Im** is more feasible than that involving the formation of **2Im**.
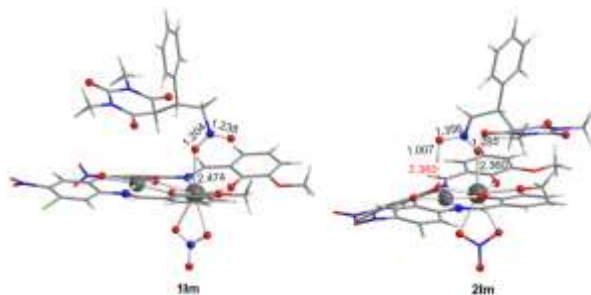
Figure 8. Equilibrium geometries of possible intermediates formed in the MA reaction of the barbiturate to *trans*-nitrostyrene catalyzed by a ZnY bimetallic catalyst

calculated at the PBE0/6-311++G(d,p) level of theory in aqueous solution.

The diastereoselectivity can be explained by considering the very loose association of the two substrates with the catalyst, where their orientation is mainly determined by maximization of the non-covalent interactions between the substrates, leading always to the formation of the R*/R* diastereoisomer irrespective of which isomer of the nitrostyrene is used. These non-covalent interactions for the catalyst-substrate complex **2Im** are shown in the SI (Figure S10). The loose association of the two substrates with the catalyst would also account for our findings using UV-Vis spectroscopy that the coordination environments of the catalyst and the catalyst+substrate are indistinguishable.

To support the proposed mechanism (Scheme 1), ESI-MS data on a sample taken during the reaction of β-methyl nitrostyrene and barbituric acid catalyzed by **1ZnGd** gave peaks with *m/z* values that support the binding of the two substrates (see SI, Figures S12-15).

CONCLUSIONS

In summary, the present study demonstrates for the first time the successful use of 3d/4f CCs as efficient catalysts for MA reactions. Although modification of the ligands in these CCs does not appear to significantly influence their structure or their catalytic properties, tuning the metal centers has provided evidence that two metal centers act cooperatively to orchestrate these rapid and highly diastereoselective reactions. DFT calculations have been used to illuminate a possible mechanism in which the CCs dissociate in solution to yield a pair of catalytically active dimers each containing a 3d and a 4f metal center. A range of spectroscopic techniques have been used to corroborate this notion. In particular, EPR studies indicate that the coordination number of both metals is unchanged in solution, confirming that the structural integrity of the dual metal scaffold remains intact and therefore able to effect cooperative catalysis. Previous studies by Shibasaki,[14,17] using 3d/4f complexes as catalysts, have employed complexes prepared *in situ*, for which no structural data either in the solid or solution states was obtained. By contrast, this current work employs structurally characterized crystalline tetrameric pre-catalysts and provides experimental evidence that these retain structural integrity in solution, albeit as 3d/4f metal containing dimers. Given the proximity of the two Lewis acidic metal centers in these structures, this supports the notion of cooperative catalysis contributing to the strong catalytic behavior they display. Future work will focus on collecting additional kinetic and spectroscopic evidence to illuminate the detailed mode of catalysis for these MA reactions and identifying new reactions for which the proximity of a tuneable pair of 3d and 4f metal centers can provide unique rate and/or selectivity characteristics.

ASSOCIATED CONTENT

Supporting Information. Experimental procedures, ES-MS, X-Ray, computational details and NMR data. This material is

available free of charge via the Internet at http://pubs.acs.org.

AUTHOR INFORMATION

Corresponding Author

*G.Kostakis@sussex.ac.uk

REFERENCES

(1) Mirica, L. M.; Vance, M.; Rudd, D. J.; Hedman, B.; Hodgson, K. O.; Solomon, E. I.; Stack, T. D. P. *Science* **2005**, *308*, 1890–1892.

(2) Kanady, J. S.; Tsui, E. Y.; Day, M. W.; Agapie, T. *Science* **2011**, *333*, 733–736.

(3) Nesterov, D. S.; Chygorin, E. N.; Kokozay, V. N.; Bon, V. V; Boča, R.; Kozlov, Y. N.; Shul'pina, L. S.; Jezierska, J.; Ozarowski, A.; Pombeiro, A. J. L.; Shul'pin, G. B. *Inorg. Chem.* **2012**, *51*, 9110–9122.

(4) Okamura, M.; Kondo, M.; Kuga, R.; Kurashige, Y.; Yanai, T.; Hayami, S.; Praneeth, V. K. K.; Yoshida, M.; Yoneda, K.; Kawata, S.; Masaoka, S. *Nature* **2016**, *530*, 465–468.

(5) Bilyachenko, A. N.; Dronova, M. S.; Yalymov, A. I.; Lamaty, F.; Bantreil, X.; Martinez, J.; Bizet, C.; Shul'pina, L. S.; Korlyukov, A. A.; Arkhipov, D. E.; Levitsky, M. M.; Shubina, E. S.; Kirillov, A. M.; Shul'pin, G. B. *Chem. Eur. J.* **2015**, *21*, 8758–8770.

(6) Ma, J. A.; Cahard, D. *Angew. Chem. Int. Ed.* **2004**, *43*, 4566–4583.

(7) Matsunaga, S.; Shibasaki, M. *Chem. Commun.* **2014**, *50*, 1044–1057.

(8) Park, J.; Hong, S. *Chem. Soc. Rev.* **2012**, *41*, 6931–6943.

(9) Buchwalter, P.; Rosé, J.; Braunstein, P. *Chem. Rev.* **2015**, *115*, 28–126.

(10) Mankad, N. P. *Chem. Eur. J.* **2016**, *22*, 5822–5829.

(11) Pye, D. R.; Mankad, N. P. *Chem. Sci.* **2017**, *8*, 1705–1718.

(12) Li, Y.; Deng, P.; Zeng, Y.; Xiong, Y.; Zhou, H. *Org. Lett.* **2016**, *18*, 1578–1581.

(13) Handa, S.; Nagawa, K.; Sohtome, Y.; Matsunaga, S.; Shibasaki, M. *Angew. Chem. Int. Ed.* **2008**, *47*, 3230–3233.

(14) Handa, S.; Gnanadesikan, V.; Matsunaga, S.; Shibasaki, M. *J. Am. Chem. Soc.* **2010**, *132*, 4925–4934.

(15) Mechler, M.; Frey, W.; Peters, R. *Organometallics* **2014**, *33*, 5492–5508.

(16) Sohtome, Y.; Kato, Y.; Handa, S.; Aoyama, N.; Nagawa, K.; Matsunaga, S.; Shibasaki, M. *Org. Lett.* **2008**, *10*, 2231–2234.

(17) Handa, S.; Gnanadesikan, V.; Matsunaga, S.; Shibasaki, M. *J. Am. Chem. Soc.* **2007**, *129*, 4900–4901.

(18) Maayan, G.; Christou, G. *Inorg. Chem.* **2011**, *50*, 7015–7021.

(19) Evangelisti, F.; More, R.; Hodel, F.; Luber, S.; Patzke, G. R. *J. Am. Chem. Soc.* **2015**, *137*, 11076–11084.

(20) Y^{III} is not a lanthanide, but has similar ionic radii to Ho^{III} and catalytic behaviour to Dy^{III}.

(21) Griffiths, K.; Gallop, C. W. D.; Abdul-Sada, A.; Vargas, A.; Navarro, O.; Kostakis, G. E. *Chem. Eur. J.* **2015**, *21*, 6358–6361.

(22) Griffiths, K.; Kumar, P.; Mattock, J. D.; Abdul-Sada, A.; Pitak, M. B.; Coles, S. J.; Navarro, O.; Vargas, A.; Kostakis, G. E. *Inorg. Chem.* **2016**, *55*, 6988–6994.

(23) Griffiths, K.; Kumar, P.; Akien, G.; Chilton, N. F.; Abdul-Sada, A.; Tizzard, G. J.; Coles, S.; Kostakis, G. E. *Chem. Commun.* **2016**, *52*, 7866–7869.

(24) Kumar, P.; Lymperopoulou, S.; Griffiths, K.; Sampani, S. I.; Kostakis, G. E. *Catalysts* **2016**, *6*, 140.

(25) Kumar, P.; Griffiths, K.; Lymperopoulou, S.; Kostakis, G. E.; Kostakis, G. E. *RSC Adv.* **2016**, *6*, 79180–79184.

(26) Hegedus, L. S. *Coord. Chem. Rev.* **2000**, *204*, 199–307.

(27) Heravi, M. M.; Hajiabbasi, P.; Hamidi, H. *Curr. Org. Chem.* **2014**, *18*, 489–511.

(28) Hamashima, Y.; Sodeoka, M. *Handbook of C-H transformations : applications in organic synthesis*; Wiley-VCH, 2005.

(29) Thirumalaikumar, M. *Org. Prep. Proced. Int.* **2011**, *43*, 67–129.

(30) Krause, N.; Hoffmann-Röder, A. *Synthesis (Stuttg).* **2001**, 171–196.

(31) Howlader, P.; Das, P.; Zangrando, E.; Mukherjee, P. S. *J. Am. Chem. Soc.* **2016**, *138*, 1668–1676.

(32) Al-Najjar, H. J.; Barakat, A.; Al-Majid, A. M.; Mabkhot, Y. N.; Weber, M.; Ghabbour, H. A.; Fun, H.-K. *Molecules* **2014**, *19*, 1150–1162.

(33) Seeliger, F.; Berger, S. T. A.; Remennikov, G. Y.; Polborn, K.; Mayr, H. *J. Org. Chem.* **2007**, *72*, 9170–9180.

(34) Griffiths, K.; Dokorou, V. N.; Spencer, J.; Abdul-Sada, A.; Vargas, A.; Kostakis, G. E. *CrystEngComm* **2016**, *18*, 704–713.

(35) Prat, D.; Hayler, J.; Wells, A. *Green Chem.* **2014**, *16*, 4546–4551.

(36) Mondal, K. C.; Sundt, A.; Lan, Y.; Kostakis, G. E.; Waldmann, O.; Ungur, L.; Chibotaru, L. F.; Anson, C. E.; Powell, A. K. *Angew. Chem. Int. Ed.* **2012**, *51*, 7550 –7554.

(37) Mondal, K. C.; Kostakis, G. E.; Lan, Y.; Wernsdorfer, W.; Anson, C. E.; Powell, A. K. *Inorg. Chem.* **2011**, *50*, 11604–11611.

(38) Irving, H.; Williams, R. J. P. *J. Chem. Soc.* **1953**, 3192.

(39) Stoll, S.; Schweiger, A. *J. Magn. Reson.* **2006**, *178*, 42–55.

(40) Misra, S. K. Multifrequency Electron Paramagnetic Resonance, Theory and Applications - Chapter 19, 2011, 1022.

(41) Wang, X.-L.; Hou, L.-L.; Zhang, J.-W.; Zhang, J.-X.; Liu, G.-C.; Yang, S. *CrystEngComm* **2012**, *14*, 3936–3944.

(42) Buckingham, D. A.; Clark, C. R.; McKeown, R. H.; Wong, O. *J. Am. Chem. Soc.* **1987**, *109*, 466–476.

(43) Delchev, V. B. *J. Struct. Chem.* **2004**, *45*, 570–578.

(44) Senthilkumar, K.; Kolandaivel, P. *J. Comput. Aided. Mol. Des.* **2002**, *16*, 263–272.

(45) Schmidt, M. U.; Brüning, J.; Glinnemann, J.; Hützler, M. W.; Mörschel, P.; Ivashevskaya, S. N.; van de Streek, J.; Braga, D.; Maini, L.; Chierotti, M. R.; Gobetto, R. *Angew. Chemie Int. Ed.* **2011**, *50*, 7924–7926.

(46) Parr, R. G.; Yang, W. *J. Am. Chem. Soc.* **1984**, *106*, 4049–4050.

(47) Ayers, P. W.; Levy, M. *Theor. Chem. Accounts Theory, Comput. Model. (Theoretica Chim. Acta)* **2000**, *103*, 353–360.

(48) Morell, C.; Grand, A.; Toro-Labbé, A. *J. Phys. Chem. A* **2005**, *109*, 205–212.

(49) Parr, R. G.; Donnelly, R. A.; Levy, M.; Palke, W. E. *J. Chem. Phys.* **1978**, *68*, 3801–3807.

(50) Kohn, W.; Becke, A. D.; Parr, R. G. *J. Phys. Chem.* **1996**, *100*, 12974–12980.

(51) Méndez, I.; Rodríguez, R.; Polo, V.; Passarelli, V.; Lahoz, F. J.; García-Orduña, P.; Carmona, D. *Chem. Eur. J.* **2016**, *22*, 11064–11083.

(52) Coles, S. J.; Gale, P. A. *Chem. Sci.* **2012**, *3*, 683–689.

TOC graphic

12
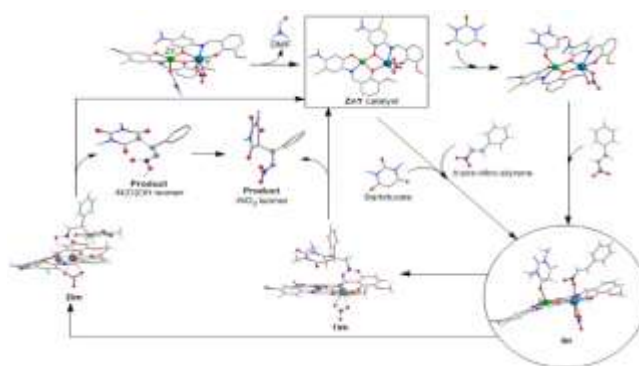
The present study demonstrates the successful use of bimetallic 3d/4f coordination clusters as efficient, cooperative and highly diastereoselective catalysts for a Michael Addition reaction.